

Radiation Feedback in Hot Accretion-Disk Corona Models

M. Böttcher, E. P. Liang, and I. A. Smith

Rice University, Space Physics and Astronomy Department, MS 108, 6100 S. Main Street, Houston, TX 77005 – 1892, USA

Received ; accepted

Abstract. We present a detailed study of the observable effects of photoionization and Comptonization of line and continuum radiation from a cold accretion disk with a thin, warm, photoionized transition layer in the framework of self-consistent accretion-disk corona models for Galactic black-hole candidates. We use an iterative method to treat the non-linear radiation feedback between the transition layer and the hot corona numerically using a Monte-Carlo Comptonization code in combination with the photoionization and line transfer code XSTAR. The subset of the parameter space allowed in self-consistent accretion-disk corona systems on energetic grounds is explored, checking for the emergence of emission lines and/or absorption edges, with special emphasis on the spectral range $E \lesssim 1$ keV where such features might become observable with the advent of the AXAF satellite. Comparing our model calculations to the broadband spectrum of GX 339-4, we find good agreement with the observed spectral features and discuss how the future detection of the predicted features at lower energies can be used to constrain parameters.

Key words: X-rays: stars — accretion, accretion disks — black hole physics — line: formation — radiative transfer — radiation mechanisms: thermal

1. Introduction

The hard X-ray and soft γ -ray spectra from Galactic black-hole candidates (GBHCs) in their low states can generally well be described by a power-law of energy index $\alpha \sim 0.4 - 0.9$ with an exponential cut-off at a few 100 keV (e. g., Grove et al. 1998). In contrast to many Seyfert galaxies, which often show evidence for a pronounced bump around $\sim 20 - 100$ keV and a strong Fe $K\alpha$ emission line at 6.4 keV (e. g., Madjejski et al. 1995, Magdziarz et al., 1997), in Galactic black-hole candidates such features are often very weak or absent. In

AGNs, they can be attributed to Compton reflection and iron fluorescence emission from a cold medium, either in a cold, optically thick outer accretion disk or in surrounding broad line regions (Lightman & White 1988, Matt et al. 1996; for a review see, e. g., Mushotzky et al. 1993).

One of the popular models to explain the high-energy spectra of GBHCs consists of a cool, optically thick accretion disk surrounded by a corona of hot, optically thin plasma (Liang & Price 1977, Bisnovatyi-Kogan & Blinnikov 1977, Haardt & Maraschi 1991, 1993). The detailed radiative transfer in a self-consistent two-phase pair corona model has been solved by Poutanen & Svensson (1996). Based on energy balance arguments, Dove et al. (1997) determined the parameter space allowed for self-consistent accretion disk corona (ADC) models, implying tight constraints on the Thomson depth τ_c and the temperature T_c of the corona, which seem to rule out a homogeneous slab geometry for the corona because the emerging spectra generally have energy spectral indices $\alpha \gtrsim 1$, inconsistent with the observed GBHC spectra.

This motivated the patchy-corona model (Haardt, Maraschi & Ghisellini 1994, Stern et al. 1995), in which the constraints on the Compton y parameter of the active regions are relaxed in the sense that these regions can be significantly hotter than a uniform slab corona, leading to spectral indices $0.5 \lesssim \alpha \lesssim 1$, depending on the local dissipation compactness in the active regions (Stern et al. 1995).

In previous analyses of ADC models for GBHCs the cold disk was generally a priori assumed to be only weakly ionized, leading to the typical Compton reflection bump, depleted by photoelectric absorption at energies $\lesssim 10$ keV, and an iron $K\alpha$ fluorescence line at 6.4 keV. However, independent studies of photoionization and fluorescence line emission (Matt et al. 1993, Zycki et al. 1994) from photoionized media have shown that the temperature and ionization structure of the cold disk very strongly influences the shape of the resulting reflection spectrum, regarding the continuum as well as line emission. These studies have also clearly demonstrated that the radiation spectrum emitted by a photoionized disk strongly differs from the thermal blackbody spectrum usually as-

Send offprint requests to: M. Böttcher

sumed as the seed photon spectrum for Comptonization in accretion-disk corona models. Given the moderate Thomson depth and Compton y parameter of the corona, $y = 4(kT_c/m_e c^2)\tau_c \lesssim 1$ for the uniform corona and $y \sim 2$ for the patchy corona case, this has significant consequences for the emerging Comptonized spectrum, particularly at low photon energies. With the advent of the AXAF satellite, line features and absorption edges in the spectra of GBHCs in the spectral range $E \lesssim 1$ keV might become observable in spite of relatively strong interstellar photoelectric absorption by neutral hydrogen.

In this work, we adopt a method similar to the one used by Zycki et al. (1994), combining the XSTAR photoionization and line transfer code (Kallman & McCray 1982) with our Monte Carlo Comptonization code in order to treat photoionization, line transfer, photoelectric absorption and Compton reflection off the disk self-consistently. Using an iterative scheme, we investigate in detail the radiation feedback between the cold disk and the hot corona, accounting for the effects of Comptonization of the cold disk emission in the hot corona and re-reflection of the Comptonized disk spectrum back onto the disk.

In Section 2, we describe the model assumptions and the numerical scheme used to treat the radiation feedback between the disk and the corona. New results of our numerical simulations are presented and discussed in Section 3. In Section 4, we demonstrate the applicability of our model calculations to the observed X-ray / soft γ -ray spectrum of GX 339-4 and make some predictions for future observations of this object. We summarize in Section 5.

2. Description of the model

For our numerical simulations of the radiation feedback between a cold accretion disk and the hot corona, we assume a plane-parallel geometry for either the entire corona (homogeneous corona) or for individual active regions (patchy corona) located above the cold disk. For the first step of our simulations, a cold disk temperature $T_d \sim 10^6$ K is used. The particle density in the cold disk is in the range $n_d \sim 10^{17} - 10^{19} \text{ cm}^{-3}$. A fraction f_c of the cold disk is sandwiched by a hot corona of Thomson depth $\tau_c \sim 0.1 - 2$ and temperature $kT_c \sim 30 - 150$ keV. Given the typical radiation temperature of the cold disk as mentioned above, Dove et al. (1997) found strict upper limits for the temperature T_c of a uniform corona, covering the entire disk, as a function of the Thomson depth. Stern et al. (1995) determined the allowed parameter space in the case of a patchy corona. The corona parameters we will adopt in our numerical simulations are chosen to be consistent with these constraints.

The details of the properties of the hot corona such as its density and temperature structure have a major influence only on the high-energy tail of the radiation spectrum. Since in this paper we are mainly interested in the

emergence of line features and absorption edges at lower photon energies, we assume for simplicity that the corona has a uniform density and temperature in accordance with the general considerations by Dove et al. (1997) and Stern et al. (1995), and defer a detailed treatment of thermal and pair balance in the corona, taking into account the spectral shape of the accretion disk radiation, to future work.

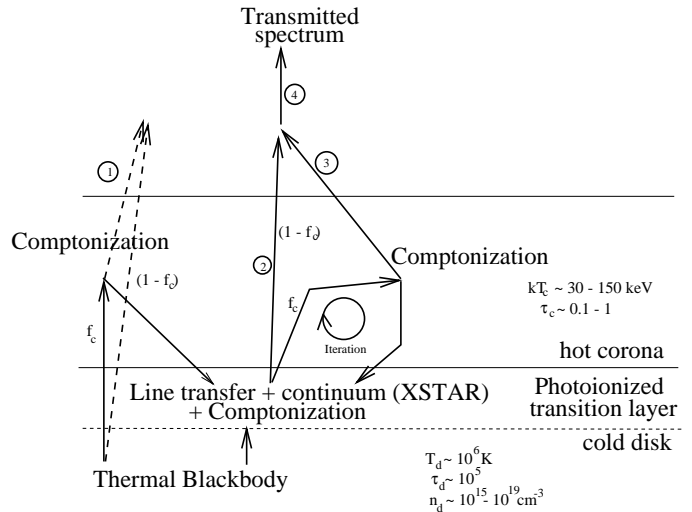


Fig. 1. Sketch of the model geometry and the iterative, numerical scheme used to treat the non-linear cold disk — hot corona feedback

The temperature and ionization structure as well as the continuum and line emissivities in the cold disk are calculated using the XSTAR code. However, since the distortion of the continuum spectrum by Compton scattering is neglected in this code, we are using our own Monte Carlo Comptonization code in order to treat Compton scattering in the photoionized surface layer of the cold disk self-consistently. The continuum radiation from the inner parts of the disk, at large Thomson depths from the disk surface, is represented by a thermal blackbody spectrum illuminating the transition layer from below.

The geometry and the iterative numerical scheme we use are sketched in Fig. 1. In the first step, we assume that the disk only emits a thermal blackbody according to our first-guess temperature of $T_d = 10^6$ K. We use an improved version of the Monte Carlo Comptonization code developed by Canfield et al. (1987) in order to simulate the processing of the disk radiation through the corona, allowing for a geometry-dependent covering fraction f_c , parametrizing the patchiness of the corona ($f_c = 1$ corresponds to the uniform slab geometry). A fraction $(1 - f_c)$ of the disk spectrum emerges directly.

We sample the transmitted spectrum as well as the spectrum of radiation reprocessed onto the cold disk. The reprocessed spectrum from the corona is used in XSTAR

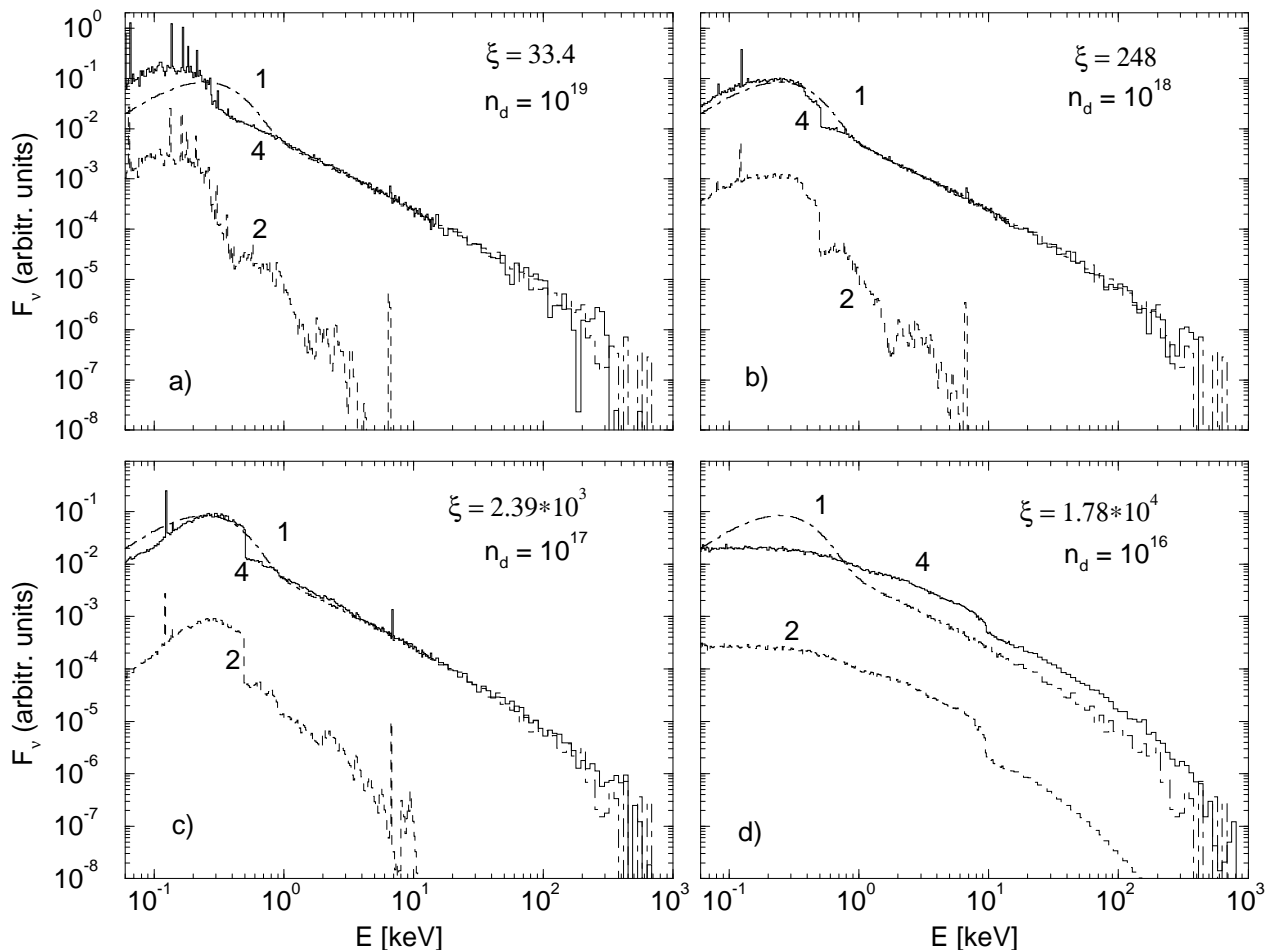


Fig. 2. The influence of the ionization parameter on the Compton reflection and line spectrum from the cold disk and the resulting total spectrum. In all panels, we used $\tau_c = 0.2$, $kT_c = 140$ keV, and $f_c = 99\%$. n_d is in units of cm^{-3} , and ξ in units of erg cm s^{-1} . The dashed curves (labeled ‘2’) show the un-Comptonized part $(1 - f_c)$ of the cold disk spectra; the solid curves (labeled ‘4’) show the total emerging spectra. For comparison, the Comptonized thermal blackbody spectra (first guess for the disk spectrum) are shown by the dot-dashed curves (labeled ‘1’)

to calculate the photoionization and temperature structure of the cold disk and the line and continuum emissivities in the disk which are used to calculate the radiation transfer due to Comptonization in the photoionized transition layer, using our Monte-Carlo code. We assume standard solar metal abundances in the cold disk.

In the second step, a fraction $(1 - f_c)$ of the new disk spectrum is processed through the corona, and again the transmitted spectrum as well as the spectrum reprocessed onto the cold disk are sampled. The reprocessed disk spectrum is then used to re-calculate the disk ionization and temperature structure and continuum and line emissivities in the disk transition layer, which are used to calculate a refined disk spectrum. This scheme is repeated iteratively until it converges to a stable output spectrum. The proper energy balance between irradiation of the cold disk by the

corona and the emission from the disk is checked a posteriori, allowing for a fraction $f_v \lesssim 0.5$ of viscous heating with respect to the total heating rate (viscous heating + irradiation by the corona) within the cold disk.

3. Numerical results and discussion

Using the radiation-feedback code described in the previous section, we explored a wide range of allowed (self-consistent) ADC model parameters. The restrictions for the corona parameters were found to be rather insensitive to the exact value of T_d (Dove et al. 1997, Stern et al. 1995). They can be characterized by the fact that for a uniform corona the Compton y parameter is restricted to $y_{\text{uniform}} \lesssim 1$ (Liang 1979), while in a strongly patchy corona $y_{\text{patchy}} \sim 2$.

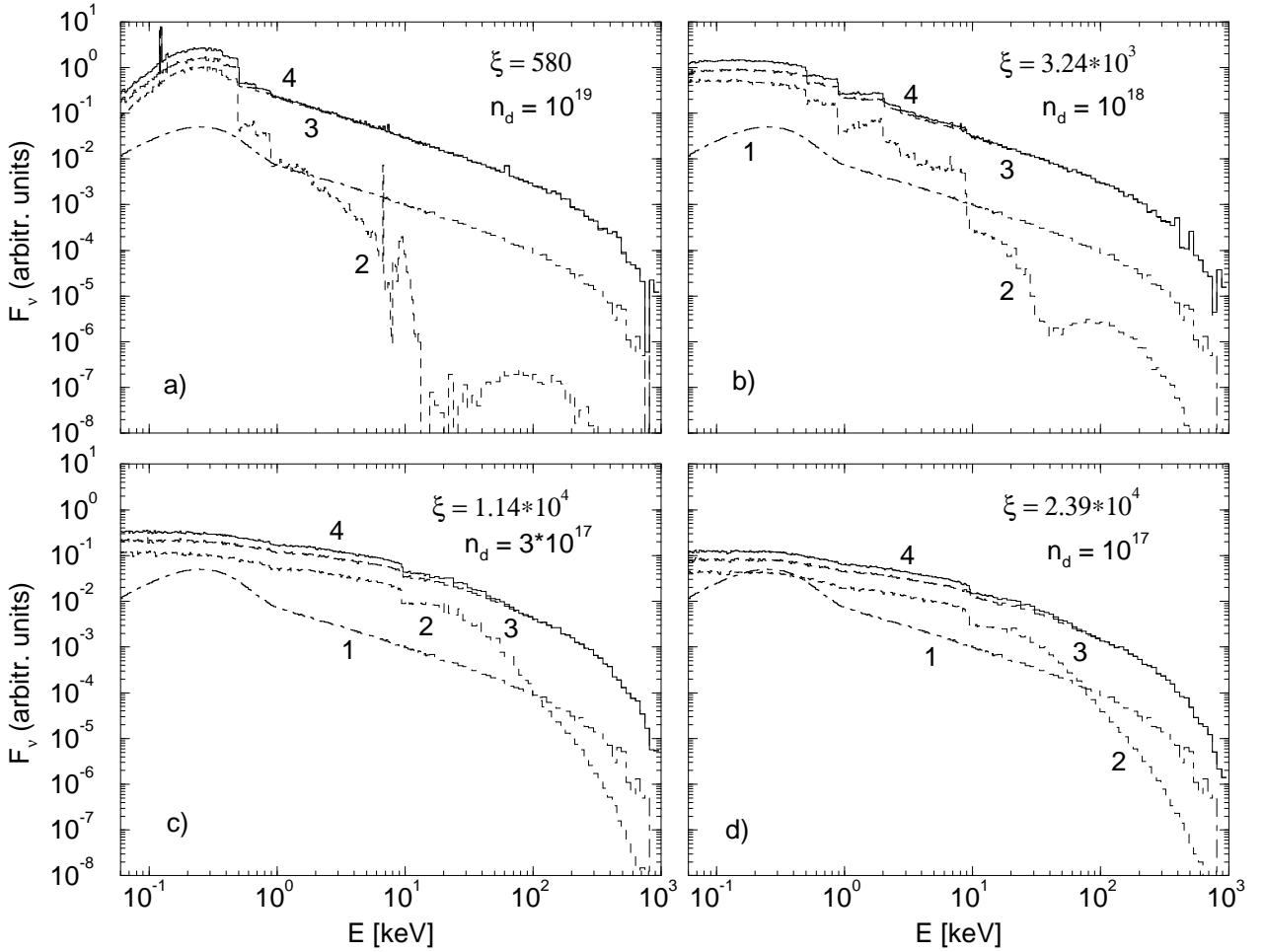


Fig. 3. Same as Fig. 2, but for covering fraction $f_c = 80\%$ and $kT_c = 100$ keV, $\tau_c = 0.5$. The long-dashed curves (labeled ‘3’) show the Comptonized disk spectrum

The ionization state of the matter in the cold disk is primarily determined by the ionization parameter

$$\xi = \frac{4\pi F_c}{n_d} \quad (1)$$

where F_c is the ionizing flux from the corona onto the disk. The effect of a varying ionization parameter, determined by a change in the assumed density of the transition layer of the cold disk, is shown in Fig. 2 where the ionization parameter is increased from $\xi = 33.3$ erg cm s $^{-1}$ (a) to $\xi = 1.78 \cdot 10^4$ erg cm s $^{-1}$ (d). The coronal parameters were chosen as $\tau_c = 0.2$ and $kT_c = 100$ keV, and the covering fraction is $f_c = 0.99$, basically corresponding to a homogeneous corona. It is important to note that ξ is not a free parameter in these simulations, but is determined self-consistently through the illumination by the corona. When varying the ionization parameter, two important trends can be observed:

(1) In agreement with the results of Matt et al. (1993), the line intensities show a maximum at a value of the ionization parameter around $\xi \sim 2000$ erg cm s $^{-1}$. Near this maximum, strong iron K and L lines as well as strong absorption edges are seen in the disk spectrum. The K line complex at 6.7 – 9 keV is almost completely smeared out by Comptonization in the corona, while the lines and absorption edges below ~ 1 keV are clearly seen in the transmitted spectrum. For significantly higher values of the ionization parameter, $\xi \gtrsim 10^4$, the fraction of completely ionized metals increases and the recombination rate decreases as a consequence of a high electron temperature, leading to a weakening of the line flux. Note that in the very-high ionization case, the dominant absorption edge is not the Fe K edge, because iron is almost fully ionized, but the Ni K edge at 8.3 keV. For $\xi \gtrsim 2 \cdot 10^4$ erg cm s $^{-1}$, emission lines become insignificant. For much lower values of ionization parameter, $\xi \ll 10^3$, photoionization becomes less im-

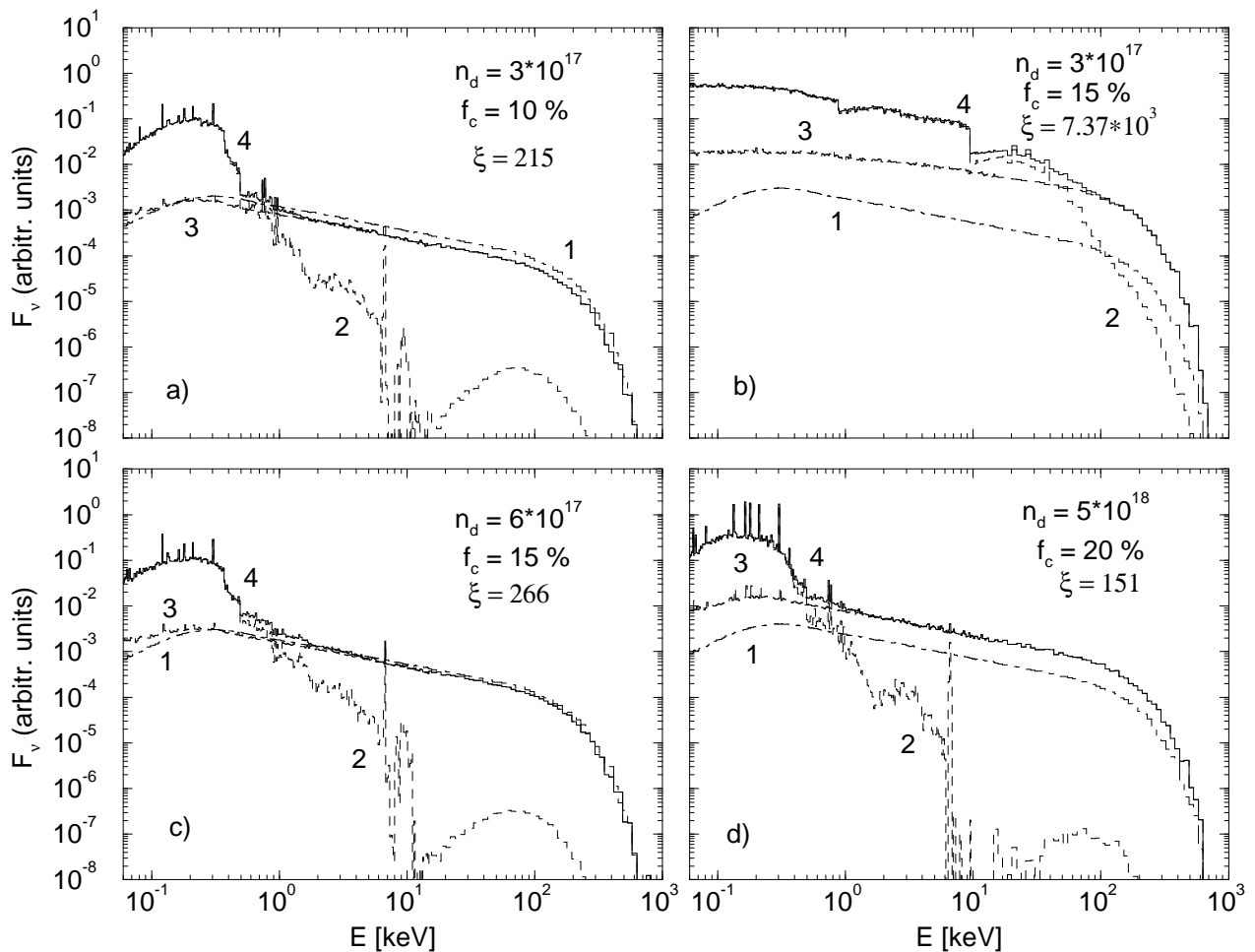


Fig. 4. Same as Fig. 3, but for low covering fractions and $kT_c = 45$ keV, $\tau_c = 2.25$.

portant, and the luminosity in fluorescence lines decreases compared to the maximum at $\xi \approx 2000$ erg cm s⁻¹.

(2) It is remarkable that for moderately ionized disks, the Compton reflection hump is very weak compared to the intrinsic disk emission, primarily due to bremsstrahlung and radiative recombination. This means that *most of the incident flux from the corona goes into heating of the disk surface layer and is not reflected*. As the ionization parameter increases, photoelectric absorption becomes less significant since an increasing fraction of the metals is highly or even completely ionized. Therefore, the Compton reflection hump becomes more luminous. In the limit of a very high ξ , the reflection spectrum does not produce the typical bump around 20 — 100 keV (depleted at lower energies by photoelectric absorption), but it is itself a power law of basically the same spectral index as the incident flux from the corona (cf. Zycki et al. 1994).

It is obvious from Fig. 2 that in the case of a large covering fraction (homogeneous corona) and a moderate ionization parameter $\xi \ll 10^3$, corresponding to disk par-

ticle densities of $n \gg 10^{17}$ cm⁻³, only a very weak iron K line feature around ~ 7 keV in the transmitted hard X-ray spectrum results, although this line is quite prominent in the disk spectrum itself.

Varying the coronal temperature T_c and Thomson depth τ_c within the allowed limits for a homogeneous corona does not alter the result described above qualitatively. With increasing Thomson depth and decreasing coronal temperature the line features emitted from the disk become more strongly smeared out in the transmitted spectrum.

Our results indicate that the Compton reflection component only results in a very weak flattening of the transmitted Comptonization spectrum with respect to thermal Comptonization of a blackbody disk spectrum. This flattening is not sufficient to resolve the $\alpha < 1$ problem of the homogeneous corona models. For low ionization parameters, $\xi \ll 10^3$, the high-energy spectrum is virtually indistinguishable from the spectrum resulting from pure Comptonization of a thermal blackbody spectrum.

Fig. 3 illustrates the effect of a varying ionization parameter with a lower covering fraction, $f = 80\%$, corresponding to a slightly patchy corona. For such a high covering fraction, the results do not deviate very much from the case $f_c = 100\%$. In the case of a very low covering fraction, $f_c \lesssim 20\%$, enabling the choice of coronal parameters consistent with the observed hard power laws with $0.5 \lesssim \alpha \lesssim 1$ in the hard X-ray range, the transition to a highly ionized disk becomes very sensitively dependent on the covering fraction for disk densities $n_d \lesssim 10^{18} \text{ cm}^{-3}$. Fig. 4 shows some examples of simulations with covering fractions in the range $10\% \leq f_c \leq 20\%$.

It should be pointed out that in the high-ionization case ($\xi \gtrsim 10^4$) a Thomson thick surface layer of the disk becomes very hot ($kT \gtrsim 10 \text{ keV}$) and therefore itself emits a hard spectrum extending up to $\sim 100 \text{ keV}$ (see Fig. 2d, 3c,d, 4b). With this type of “soft” seed photon spectrum, the considerations regarding the energy equilibrium in the corona become invalid since these were based on a soft blackbody spectrum of temperature $\sim 10^6 \text{ K}$. A self-consistent treatment of this case therefore requires the detailed re-consideration of heating and cooling processes in the corona, using the exact disk spectrum, which we defer to future work. The results presented here may be regarded as reliable only in the case of moderate ionization of the disk ($\xi \lesssim 2000 \text{ erg cm s}^{-1}$).

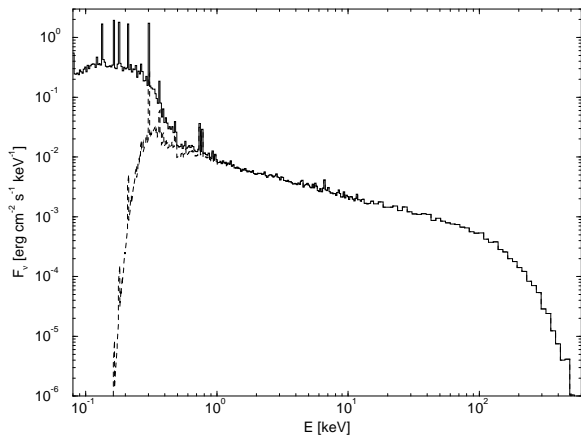


Fig. 5. The total disk corona spectrum of Fig. 4d (solid), corrected for photoelectric absorption by neutral ISM or CSM hydrogen, $N_H = 5 \cdot 10^{21} \text{ cm}^{-2}$ (dashed).

As mentioned above, only in the patchy-corona model, invoking Thomson thick active regions, the observed hard power-laws of the Comptonization continuum can be produced self-consistently. A second argument for the patchy corona are the observed uncorrelated variability patterns of the hard power-law component and the soft (cold disk)

radiation component, which cannot be understood in the framework of a corona model with $f_c \sim 100\%$.

Our results confirm that the exact spectrum of the cold disk has negligible influence on the hard power-law portion of the X-ray spectrum. However, below $\sim 1 \text{ keV}$, strong emission lines from mildly to highly ionized metals may arise, depending on the ionization parameter and the spectrum of the ionizing continuum, incident from the corona. However, at these energies the X-ray flux from any source near the galactic plane will be heavily absorbed by neutral hydrogen. To illustrate this, we plot in Fig. 5 the total AD corona spectrum of Fig. 4d, corrected for photoelectric absorption by a hydrogen column density of $N_H = 5 \cdot 10^{21} \text{ cm}^{-2}$, which we estimate to be the actual N_H toward GX 339-4. It becomes obvious that only down to $\gtrsim 0.3 \text{ keV}$, emission line features would be detectable by observing instruments sensitive in this energy range.

4. Application to GX 339-4

In 1996, we performed a series of multiwavelength observations of the galactic black hole candidate GX 339-4 (Smith et al. 1998a, Smith & Liang 1998, Smith et al. 1998b). GX 339-4 is unusual in that it is a persistent source, being detected by X-ray telescopes most of the time, but it also has nova-like flaring states. Our observations were made when the source was in a persistent hard state (= soft X-ray low state).

As part of this campaign, we performed a pointed observation 1996 July 9-23 using the Oriented Scintillation Spectrometer Experiment (OSSE) on the *Compton Gamma-Ray Observatory* (CGRO). A pointed observation was also made using the *Rossi X-Ray Timing Explorer* (RXTE) 1996 July 26 (MJD 50290), just after the OSSE run ended. Full details of the observations, the extraction of the spectra, and fitting of the spectra using simple phenomenological models is given in Smith et al. (1998a).

We generated the RXTE spectrum using two of its instruments, the Proportional Counter Array (PCA), and the High Energy X-ray Timing Experiment (HEXTE). Our RXTE observations showed that the emission was extremely variable, with the 2–5 keV band being slightly more variable than the 10–40 keV band (Smith & Liang 1998). However, the hardness ratio showed no correlation with time during the observation, and so we averaged all the RXTE data to generate a spectrum that is representative of its shape throughout the run. Both a power law times exponential (PLE) and a Sunyaev-Titarchuk (ST; Sunyaev & Titarchuk 1980) function fit the spectrum above $\sim 15 \text{ keV}$. An additional soft component is required, as well as a broad emission feature centered on $\sim 6.4 \text{ keV}$ whose equivalent width is $\sim 600 \text{ eV}$. No reflection component is required to fit the spectrum.

The OSSE spectrum was extracted by averaging over the whole two week observation. Since the hardness ratio did not change significantly over this time, this again gives

a reliable measure of the spectral shape. Both a PLE and a ST model also fit our OSSE spectrum on its own.

We combined the *RXTE* and OSSE data to generate the joint spectrum. The results should be treated with care, because the two data sets are not quite simultaneous, and the source is highly variable. However, since the hardness ratios did not change dramatically in either observation, the resulting spectral shape is a good representative average of the source in 1996 July. We found that the PLE model easily fits the joint spectrum. However, the ST model has too much curvature to give an acceptable joint fit.

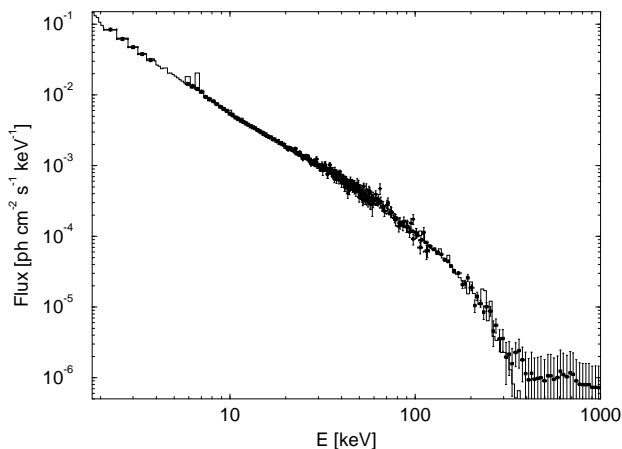


Fig. 6. Joint *RXTE*–OSSE spectrum and PLE model fit for 1996 July observations of GX 339–4. Note that the two data sets are not quite simultaneous, and the source is highly variable, so this figure should be used with care. The data have been unfolded using a PLE model with a power law for the soft component plus a Gaussian line and an edge. The histogram shows a fit by eye using our detailed corona model.

Figure 6 shows the unfolded data using a PLE fit. The PCA, HEXTE, and OSSE data have been normalized as described in Smith et al. (1998a). In the PLE model, the flux has the form $F(E) \propto E^{-\alpha} \exp(-E/kT)$, and the best fit values were $\alpha = 1.22 \pm 0.01$ and $kT = 96.9$ keV (fixed by the OSSE data). In addition to the PLE, the soft component is a power law with photon index 3.00 ± 0.06 and $N_H = 5 \times 10^{21} \text{ cm}^{-2}$ (fixed from the *EXOSAT* observations that more reliably measured the lower energy spectrum (Ilovaisky et al. 1986, Méndez & van der Klis 1997)). A Gaussian line is added, with centroid 6.6 ± 0.3 keV and width $\sigma = 1.7 \pm 0.1$ keV, and an edge with threshold energy 7.18 ± 0.08 keV and absorption depth 0.09 ± 0.02 at the threshold is included. (The errors are 90 % confidence regions for varying one parameter.) This fit has reduced $\chi^2_{\nu} = 1.025$. The probability that a random set of data

points would give a value of χ^2 as large or larger than this is $Q = 0.36$.

Our detailed model is highly non-linear and cannot be written as a simple parametrization. We are therefore currently unable to directly fit the observations using the normal forward folding χ^2 minimization techniques. Eventually we aim to build a library of spectra generated for ranges of parameters of interest, and then be able to perform the fitting from these. In this paper, we restrict ourselves to fitting by eye the unfolded spectrum obtained from a PLE best fit model to illustrate that our model gives realistic results.

The histogram in Figure 6 shows a realistic model calculation using our detailed corona model. The parameters used are $\tau_c = 2.2$, $kT_c = 44$ keV, $f_c = 18\%$, $n_d = 5 \cdot 10^{17} \text{ cm}^{-3}$ with the resulting ionization parameter $\xi = 516 \text{ erg cm s}^{-1}$. The continuum shape over the entire energy range of the observation is very well described by our model calculation. However, since we neglected the effects of line broadening due to Keplerian rotation and turbulent motion in the disk, the model Fe K α line is narrower than observed. Although the line width is not accurately modeled by our calculation, Fig. 6 indicates that, in addition to the hard power-law and the exponential cutoff, the soft power-law at low energies as well as the iron edge, required by the phenomenological fit to the data, are well reproduced by our model.

In agreement with the phenomenological fit, the reflection component resulting from our model calculation is negligible. Our simulations show that this is a natural consequence of the moderate ionization of the surface layer of the disk.

The absence of a strong reflection component is also in agreement with the analysis of observations of Cyg X-1 by Dove et al. (1998) two weeks after a transition to its hard (low) state, using a broadband spectrum covering the entire 3 – 200 keV energy range. These authors argue that the strong Compton reflection component usually seen in the low state of Cyg X-1 might in part be an artifact due to the incomplete frequency coverage of previous observations of Cyg X-1. Restricting their analysis to the 3 – 30 keV and 100 – 200 keV ranges, they find a best fit including a relatively strong Compton reflection component corresponding to a covering fraction $f = 0.35 \pm 0.02$ of a cold disk intercepting the hard power-law emitted by the corona. This is in agreement, e. g., with the results of Gierliński et al. (1997) who used Ginga + OSSE observations, covering approximately the energy range mentioned above.

If the value of $N_H = 5 \cdot 10^{21} \text{ cm}^{-2}$ for the galactic hydrogen column density towards GX 339-4, which we assumed in unfolding the observed spectrum, is realistic, our calculations predict that future observations of this object in the energy range $\sim 0.3 - 1$ keV, which will become possible with the advent of the AXAF mission, should reveal significant emission lines and/or absorption edges from the

photoionized disk which will be extremely useful to further constrain the ionization state of the disk surface and thereby the geometry. The model calculation shown in Fig. 6 predicts the presence of strong Fe L and Ni L edges at 0.7 and 0.8 keV and a strong O L edge at 0.5 keV. These predictions, in turn, can be used to determine the hydrogen column density towards the source more precisely.

5. Summary and conclusions

We have developed a method to treat self-consistently the radiation feedback between a cold accretion disk and a homogeneous or patchy, hot corona surrounding the disk. The detailed shape of the disk radiation spectrum, strongly deviating from a blackbody spectrum, has consequences especially for the observable X-ray spectrum below a few keV. Above this energy, the Comptonization spectra are virtually indistinguishable from thermal Comptonization of a soft blackbody spectrum.

Accounting for the exact thermal and ionization balance, using the XSTAR code, we find that due to the usually moderate ionization of the surface layer of the cold disk, the reflection component is in most cases negligible. This is in accord with recent results that the broadband X-ray and soft γ -ray spectra of GX 339-4 and Cyg X-1 can be well fitted with a pure power-law + exponential cutoff, without a Compton reflection component.

Our model calculations predict the existence of strong emission lines and/or absorption edges at energies $\lesssim 1$ keV, which are usually hard to observe because of strong absorption by neutral hydrogen. However, with the advent of the AXAF satellite with its unprecedented sensitivity at low X-ray energies, it might become possible to test the predictions of our calculations and use the results to determine the ionization parameter of the disk surface layer and the covering fraction of the corona with respect to the cold disk. Given that the coronal temperature and Thomson depth can usually be well constrained by the hard power-law index and the cut-off energy at hard X-ray / soft γ -ray energies, knowledge of the disk surface ionization state and the covering fraction would allow a detailed study of the structure of the accretion disk.

Acknowledgements. We thank T. Kallman for advice regarding the XSTAR code. This work was supported by NASA grants NAG 5-4055, NAG 5-1547, and NAG 5-3824 at Rice University.

References

- Bisnovatyi-Kogan, G. S., & Blinnikov, S. I., 1977, A&A, 59, 111
- Canfield, E., Howard, W. M., & Liang, E. P., 1987, ApJ 323, 565
- Dove, J. B., Wilms, J., & Begelman, M., 1997, ApJ 487, 747
- Dove, J. B., Wilms, J., Nowak, M. A., et al., 1998, MNRAS, in press
- Gierliński, M., Zdziarski, A. A., Done, C., et al., 1997, MNRAS, 288, 958
- Grove, J. E., Johnson, W. N., Kroeger, R. A., et al., 1998, ApJ 499
- Haardt, F., & Maraschi, L., 1991, ApJ 380, L51
- Haardt, F., & Maraschi, L., 1993, ApJ, 413, 507
- Haardt, F., Maraschi, L., & Ghisellini, G., 1994, ApJ 432, L95
- Ilovaisky, S. A., Chevalier, C., Motch, C., & Chiappetti, L. 1986, A&A, 164, 67
- Kallman, T. R., & McCray, R. A., 1982, ApJS 50, 263
- Liang, E. P., 1979, ApJ, 231, L111
- Liang, E. P., & Price, R. H., 1977, ApJ, 218, 247
- Lightman, A. P., & White, T. R., 1998, ApJ 355, 57
- Madejski, G. M., Zdziarski, A. A., Turner, T. J., et al., 1995, ApJ 4838, 672
- Magdziarz, P., Blaes, O., Zdziarski, A. A., et al., 1997, in 4th Compton Symposium, Eds. Dermer, C. D., Strickman, M. S., & Kurfess, J. D., 1997, p. 1288
- Matt, G., Fabian, A. C., & Ross, R. R., MNRAS 262, 179
- Matt, G., Brandt, W. N., & Fabian, A. C., MNRAS 280, 823
- Méndez, M., & Van der Klis, M. 1997, ApJ, 479, 926
- Mushotzky, R. F., Done, C., & Pounds, K. A., 1993, Ann. Ref. Astron. Astroph. 31, 717
- Poutanen, J., & Svensson, R., 1996, ApJ 470, 249
- Smith, I. A., et al. 1998, ApJ, submitted
- Smith, I. A., & Liang, E. P. 1998, ApJ, submitted
- Smith, I. A., Filippenko, A. V., & Leonard, D. C. 1998, ApJl, submitted
- Stern, B. E., Poutanen, J., Svensson, R., et al., 1995, ApJ 449, L13
- Sunyaev, R. A., & Titarchuk, L. G. 1980, A&A, 86, 121
- Zycki, P. T., Krolik, J. H., Zdziarski, A. A., & Kallman, T. R., 1994, ApJ 437, 597